DOE/ER/13695--T1

DOE/ER/13695--T1

DE90 002873

A **Progress Report** for 1988-1989

to the

DEPARTMENT OF ENERGY

Attn: Dr. William Kirchoff
Program Manager, Chemical Physics
Division of Chemical Sciences
Office of Basic Energy Sciences
US Department of Energy
ER-616 Mail Stop J-309 GTN
Washington, DC 20545
(301) 353-5820

Support by

LASER PHOTOELECTRON SPECTROSCOPY OF IONS

(Grant DE-FG02-87ER13695)

October, 1989

Name and Address of Institution:

The Regents of the
University of Colorado
Campus Box B-19
Boulder, Colorado 80309

Principal Investigator:

G. Barney Ellison
Department of Chemistry
& Biochemistry
University of Colorado
Boulder, CO 80309-0215

G B. Ellison

We use photoelectron spectroscopy to study the properties of negative ions and radicals. The essence of our experiment is to cross a 0.6 keV mass-selected ion beam (M^-) with the output of a CW laser, $\hbar\omega_o$. The resultant detached photoelectrons with kinetic energy, KE, are energy analyzed by means of a set of electrostatic hemispherical analyzers.

$$M^- + \hbar\omega_o \rightarrow M + e(KE)^-$$

Analysis of the photoelectron spectra enables us to extract molecular electron affinities, vibrational frequencies and electronic splittings of the final radical, M, as well as the relative molecular geometries of ions (M^-) and radicals (M).

During the last three years we have completed the several studies: (1) borane, (2) amide, (3) oxygen and nitric oxide, and (4) ethylene and acetylene. We have also nearly compelted a major overhaul of our photoelectron spectrometer that will permit us to prepare collisionally relaxed ions in a flowing afterglow ion source.

II. Progress

A. Spectroscopy of Reactive Intermediates

1. Photoelectron Spectroscopy of the Borane Ion

We have studied[1] the photoelectron spectra of BH_3^- and BD_3^- and have measured the electron affinities of borane; we find EA(BH_3) = 0.039 ± 0.015 eV and EA (BD_3) = 0.027 ± 0.014 eV. The peak splittings and intensities demonstrate that the BH_3^- ion and the BH_3 neutral have very similar geometries; our spectra are consistent with a planar structure for both species. Variational calculations of a coupled oscillator basis over an *ab initio* potential give an excellent fit to the experimental frequencies and photodetachment Franck Condon factors. This *ab initio* model leads to equilibrium geometries with both

BH_3 and BH_3^- as planar molecules with $r_e(BH_3^-) = 1.207$ Å and $r_e(BH_3) = 1.188$ Å. We find $\Delta H^o_{f0}(BH_3^-) = 23.1 \pm 3.8$ kcal/mol.

The negative ion photoelectron spectra reveal a Franck Condon profile with an intense (0,0) feature and a much weaker (1,0) band. A variational calculation of vibrational states shows that this exited state is in fact a pair of states which are mixed by a Fermi resonance between the fundamental of the symmetric stretch, $\upsilon_1 = 1$, and the first overtone of the out-of-plane bend, $\upsilon_2 = 2$. While the weight of evidence in our study both from Franck Condon calculations and from *ab initio* calculations of the geometry of the ion shows it to be planar, we cannot state this with complete certainty. However we can say that an ion bent out of the plane by more than 7° is highly inconsistent with our experiments.

2. Photoelectron Spectroscopy of the Amide Ion

We report[2] the electron affinity of amidogen (NH_2), the amino radical, obtained from the photoelectron spectrum of the amide ion, NH_2^-. The literature electron affinity values from early laser photodetachment experiments have relative large uncertainties, $EA(NH_2) = 0.744 \pm 0.022$ eV from photodetachment threshold measurements[3] and $EA(NH_2) = 0.779 \pm 0.037$ eV from photoelectron spectroscopy.[4] The development of higher resolution (5-25 meV) negative ion photoelectron spectrometers now permits a significantly improved determination of the electron affinity as well as the observation of more detailed structure in the photoelectron spectrum. The spectrum reported here shows clear rotational bands in the photodetachment of NH_2^-. The rotationaless origin is found from rotational modeling to be within 1 meV of the center of the Q band and this yields the electron affinity, $EA(NH_2) = 0.771 \pm 0.001$ eV. We have also measured the angular distribution of the ejected electron with the laser operating on the 351 nm line. This showed anisotropic detachment with asymmetry parameter β of 0.34 ± 0.05. Within experimental error the Q, P, and R branches all had the same angular distribution.

3. Electron Affinities of Oxygen and Nitric Oxide

A pair of important species in combustion processes are O_2 and NO. Our current spectrometer, with its increased sensitivity and resolution, gives raw electron affinities for nitric oxide and oxygen 10 to 20 meV higher than earlier reported.[5,6] We have re-examined[7] the photoelectron spectra of O_2^- and NO^- using negative ion photoelectron spectroscopy. We observe (Fig. II.3) detachment to three electronic states ($^3\Sigma_g^-$, $^1\Delta_g$, $^1\Sigma_g^+$) of O_2 and to one electronic state ($^2\Pi$) of NO. We find the following electron affinities: $EA(O_2) = 0.451 \pm 0.007$ eV and $EA(NO) = 0.026 \pm 0.005$ eV. Analyses of the photoelectron spectra yield a value for the fundamental frequency of O_2^- (1073 ± 50 cm^{-1}) while the bond lengths are $r_e(O_2^-) = 1.347 \pm 0.005$ Å and $r_e(NO^-) = 1.271 \pm 0.005$ Å. These results now supercede the earlier pioneering photodetachment spectra.[2,3]

4. Bond Strengths of Ethylene and Acetylene

One of the more interesting properties of a molecule is the strength of each of the bonds.[8] But there are not many molecules larger than triatomics for which all of the bond dissociation energies are known; methane,[9] silane,[10a] germane,[3b] ammonia,[3c] phosphine,[3c] and arsine[3c] are cases that have been worked out. We have used gas phase ion chemistry and photoelectron spectroscopy to report all of the bond strengths of CH_2=CH_2 and HC≡CH.

Modern ion chemistry and spectroscopy provide a powerful avenue by which bond strengths can be established. Our method is to use negative ion photoelectron spectroscopy to measure the radical electron affinity, EA(R), the enthalpy change for process (1),

$$R^- \rightarrow R + e^- \qquad (1)$$

in conjunction with proton transfer reaction kinetics to determine of the hydrocarbon gas phase acidity, $\Delta H^o_{acid}(RH)$, the enthalpy change for process (2).

$$R\text{-}H \rightarrow R^- + H^+ \qquad (2)$$

These values are combined to extract the homolytic bond dissociation energy.[11,12]

$$D_0(RH) = \Delta H^o_{acid}(R\text{-}H) + EA(R) - IP(H) \quad (3)$$

where IP(H) = 313.59 kcal/mol is the ionization potential of the hydrogen atom.[13]

We have established[14] the gas phase acidities of $CH_2{=}CH_2$, $CH_2{=}CH$, and HC≡CH by proton transfer kinetics in a flow tube reactor. Separate measurements in a photoelectron spectrometer provide electron affinities for $CH_2{=}CH$, $CH_2{=}C$, and HC≡C. These values are used in (3) to determine the hydrocarbon bond strengths, $D(CH_2CH\text{-}H)$, $D(CH_2C\text{-}H)$, and D(HCC-H). Together with established heats of formation for related species, these experimental values enable us to derive all of the other bond dissociation energies in acetylene and ethylene. We find the CH bond dissociation energies of acetylene, ethylene and vinyl radical: $D_0(HCC\text{-}H) = 131.6 \pm 0.6$ kcal/mol, $D_0(CH_2CH\text{-}H) = 109.7 \pm 0.8$ kcal/mol, and $D_0(CH_2C\text{-}H) = 80.0 \pm 5.0$ kcal/mol. The strengths of each of the other CH and CC bonds in acetylene and ethylene and their fragments are derived. The rearrangement of acetylene is an important reaction.

$$HC{\equiv}CH \rightarrow CH_2{=}C \quad (4)$$

The isomerization energy of acetylene (I) to vinylidene (II) is found: $\Delta H^o_0(I \rightarrow II) = +46.4 \pm 5.5$ kcal/mol. As part of this bond strength study, proton transfer kinetics in a flowing afterglow device have been used to refine the acidities of acetylene and ethylene. The gas phase acidity of ethylene, acetylene, isopropyl alcohol and *tert*-butyl alcohol have been directly tied to ammonia and hydrogen fluoride, both of which are very precisely known: $\Delta G^o_{acid}(NH_3) = 396.5 \pm 0.4$ kcal/mol and $\Delta G^o_{acid}(HF) = 365.6 \pm 0.2$ kcal/mol. We fix these acidities as follows: $\Delta G^o_{acid}(CH_2CH\text{-}H) = 401.0 \pm 0.5$ kcal/mol, $\Delta G^o_{acid}(HCC\text{-}H) = 369.7 \pm 0.3$ kcal/mol, $\Delta G^o_{acid}((CH_3)_2CHO\text{-}H) = 370.0 \pm 0.3$ kcal/mol, and $\Delta G^o_{acid}((CH_3)_3CO\text{-}H) = 369.2 \pm 0.3$ kcal/mol.

The results of our experimental studies are collected together in Chart I. This tableau shows the dissociation energies of CH_2=CH_2 and HC≡CH into *all* possible fragments. While discrepancies with other experimental determinations of the ethylene and acetylene CH bond strengths remain, the general trends shown in Chart I are certain. It is particularly important to note that methane, ethylene, and acetylene are among the simplest set of hydrocarbons with sp^3, sp^2, and *sp* carbon atoms. The set of energies, $D_o(CH_3\text{-H})$ = 103.24 ± 0.12 kcal/mol[15] < $D_o(CH_2CH\text{-H})$ = 109.7 ± 0.8 kcal/mol < $D_o(HCC\text{-H})$ = 131.6 ± 0.6 kcal/mol, is a very important one to establish.

CHART I
Experimental Bond Strengths

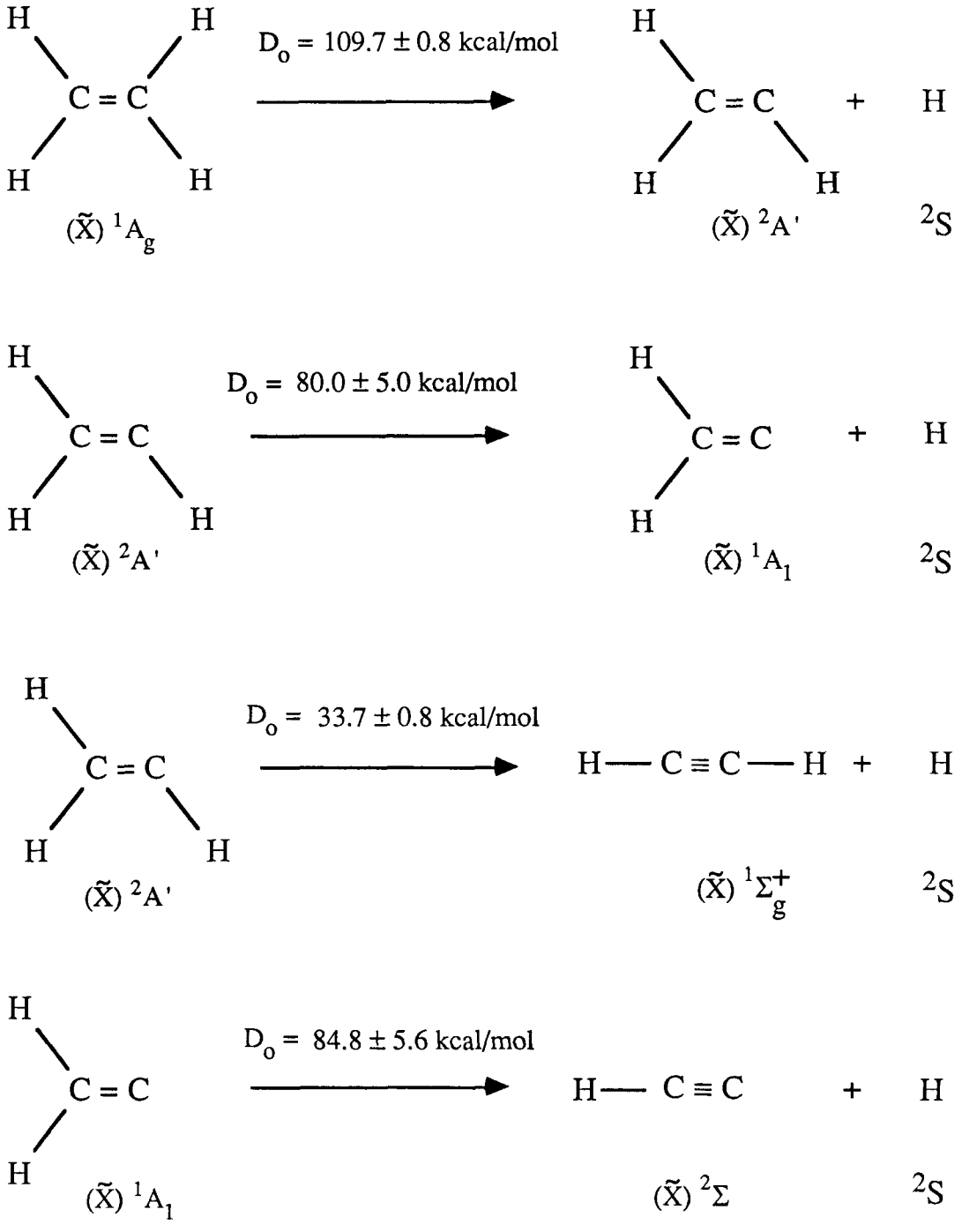

$D_o = 131.1 \pm 0.4$ kcal/mol

$$H{-}C{\equiv}C{-}H\ (\tilde{X})\ {}^1\Sigma_g^+ \longrightarrow H{-}C{\equiv}C\ (\tilde{X})\ {}^2\Sigma + H\ {}^2S$$

$D_o = 116.5 \pm 1.0$ kcal/mol

$$H{-}C{\equiv}C\ (\tilde{X})\ {}^2\Sigma \longrightarrow C{\equiv}C\ (X)\ {}^1\Sigma_g^+ + H\ {}^2S$$

$D_o = 228.8 \pm 0.7$ kcal/mol

$$H{-}C{\equiv}C{-}H\ (\tilde{X})\ {}^1\Sigma_g^+ \longrightarrow H{-}C\ (X)\ {}^2\Pi + C{-}H\ (X)\ {}^2\Pi$$

$D_o = 177.5 \pm 0.6$ kcal/mol

$$H{-}C{\equiv}C\ (\tilde{X})\ {}^2\Sigma \longrightarrow H{-}C\ (X)\ {}^2\Pi + C\ {}^3P$$

$D_o = 140.9 \pm 0.9$ kcal/mol

$$C{\equiv}C\ (X)\ {}^1\Sigma_g^+ \longrightarrow C\ {}^3P + C\ {}^3P$$

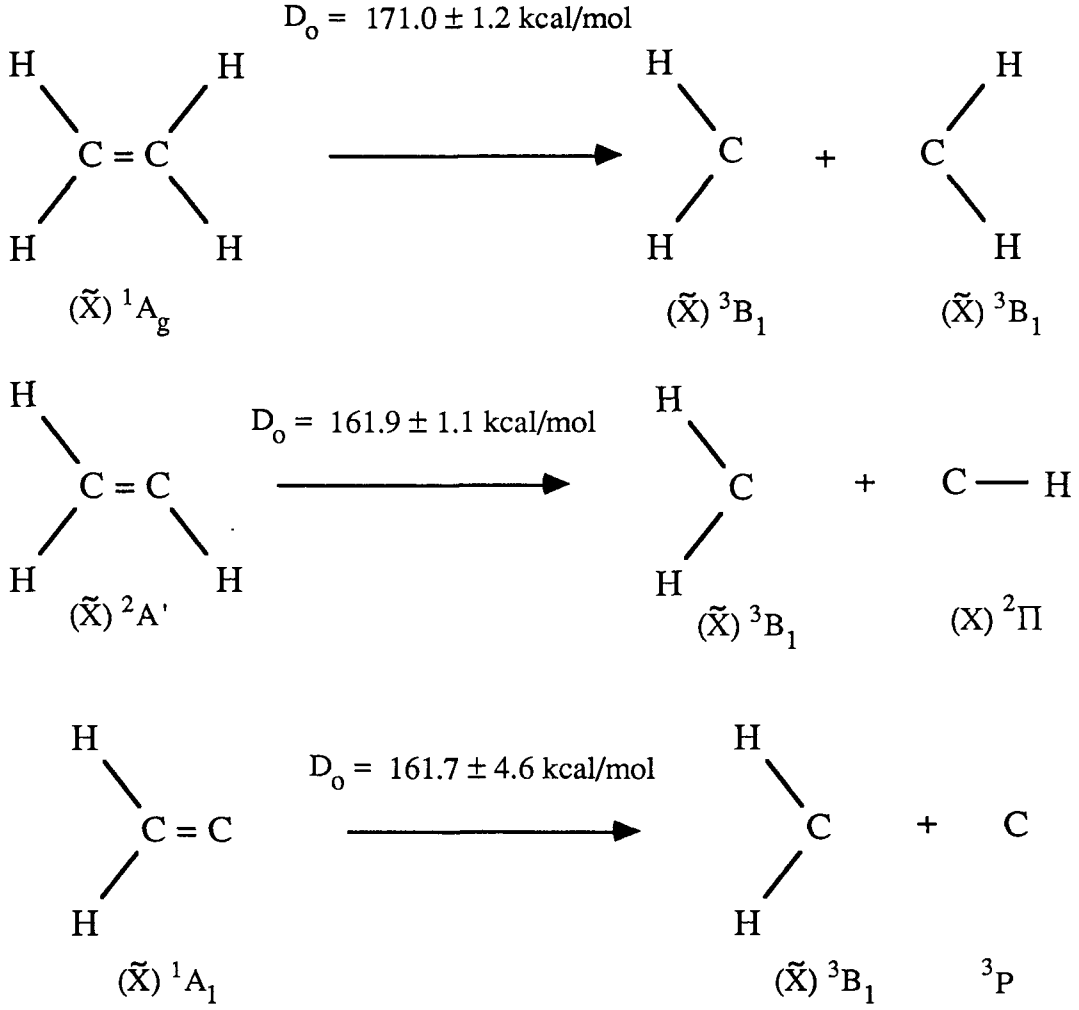

B. Instrumentation

1. Experimental Overview

In the last several years we have made substantial modifications to our photoelectron spectrometer to dramatically improve its performance. In this section, we review the current photoelectron spectrometer, discuss its shortcomings, and describe several improvements that we have implemented. During the last three years, we have designed and fabricated a totally new hemispherical electron energy analyzer. The new

analyzer, together with a flowing afterglow ion source and a new high resolution Wien filter are built and are now being assembled.

Our original photoelectron spectrometer has been described in detail elsewhere.[16,17] Briefly, we prepare negative ions in a high pressure (0.1 Torr), DC plasma discharge; the ions are extracted, formed into a beam and accelerated to 600 eV. The beam is then velocity selected with a 6 in. Wien filter. This mass selected beam, with a typical magnitude of 1 nA, is then delivered to a high vacuum chamber (10^{-9} Torr) where it intersects the output of a CW Ar II laser operating on a single line. The laser operates in an intracavity mode and generates about 75 W of circulating power on the λ_o = 488 nm line. A portion (10^{-3}) of the scattered electrons is collected and analyzed by a pair of 1 in. mean radius hemispherical deflectors operating in series.

Our current spectrometer has several shortcomings. (a) Ions produced in the extremely energetic plasma discharge can have high vibrational temperatures in the range of 500-1200 ^{o}K. Fragile, collisionally relaxed ions can be prepared by using a flowing afterglow ion source but instead of nA beam currents, an afterglow ion source only delivers ion currents about 1000 smaller than our standard plasma discharge source. (b) The low sensitivity of our electron energy analyzer has stymied the installation of our flowing afterglow ion source. Our original analyzer requires approximately 100-200 pA ion beam currents to produce a spectrum. We had hoped to ameliorate this by replacing the channeltron multiplier with a position-sensitive detector and gain a factor of about 50 in sensitivity. Unfortunately we could find no improvement at all in the spectrometer's sensitivity. (c) Our 6 in. Wien filter has a mass resolution ($\frac{M}{\Delta M}$) of only 90 so we are restricted to the study of ions with m/z less than 100. (d) The highest energy laser line that we can access is only 488.0 nm. Because of these deficiencies, our studies are confined to small, vibrationally excited ions whose electron affinities are 2.540 eV or less.

2. <u>New Spectrometer</u>

In order to address some of the limitations of our current instrument, we have designed and are now completing the fabrication of a totally new photodetachment spectrometer, Fig. 1.

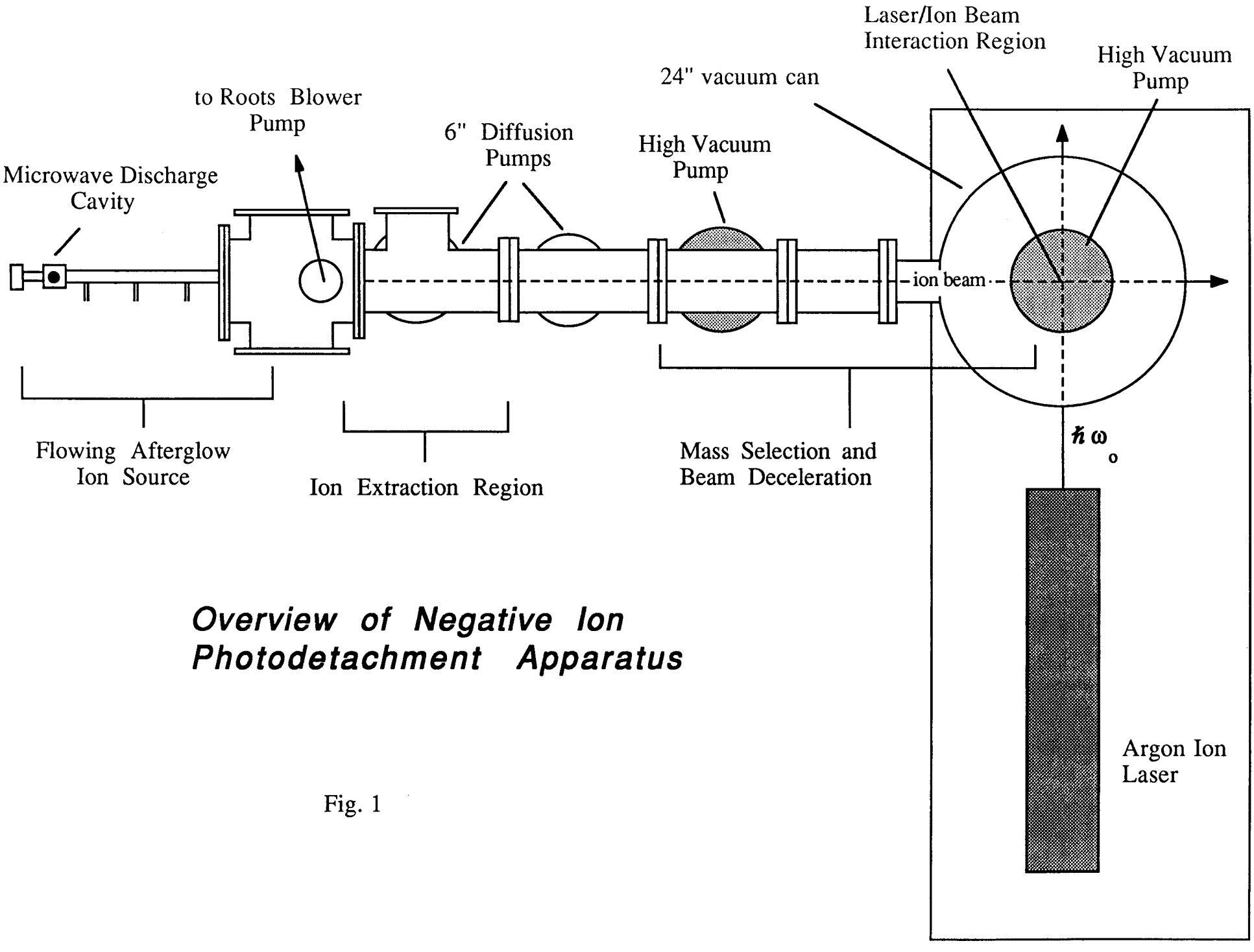

Overview of Negative Ion Photodetachment Apparatus

Fig. 1

This state-of-the-art device incorporates several high performance components. (a) It utilizes a flowing afterglow device as a source of collisionally-relaxed ions. (b) The mass-selection device, the Wien filter, is fitted with a 1.5 m flight tube that extends its mass resolution to roughly 500. (c) It incorporates a totally new 6 in. diam. hemispherical analyzer with sensitivity and resolution capabilities far superior to those of the old analyzer. The flowing afterglow device, Wien velocity filter, and new electrostatic analyzer will be reviewed.

(i) Flowing Afterglow Ion Source

Flowing afterglow ion sources are by now standard devices.[18] We generate precursor ions in a 2540 MHz discharge generated with a 2 in. Evenson cavity.[19] Ion precursors are entrained in a fast flow of He buffer gas ($\frac{1}{2}$ Torr) and react with injected reagent gases as they traverse a short length of 1.5 in. glass tubing. The flow velocity (80 m/sec) is maintained by a 600 L/sec Roots blower. Ions in this environment tend to be vibrationally relaxed by roughly 10^4 collisions with the He buffer gas. With this device, we can select from the vast number of tabulated ion-molecule reactions to create an ion of choice. For example, the fragile peroxide ion $CH_3O_2^-$ can be easily created in a flowing afterglow by proton abstraction,[20]

$$CH_3O_2H + NH_2^- \rightarrow CH_3O_2^- + NH_3 \qquad (7)$$

Attempts to make peroxide anions in a plasma discharge ion source always fail; introduction of CH_3O_2H into a standard Branscomb source gives CH_3O^- and OH^- only.

It is possible to make high concentrations of ions in a flowing afterglow device. Direct measurements with a Langmuir probe[21] indicate that one can attain ion densities of 10^{10} cm^{-3}. Ions are extracted from the afterglow by a nosecone as shown in Fig. 2.

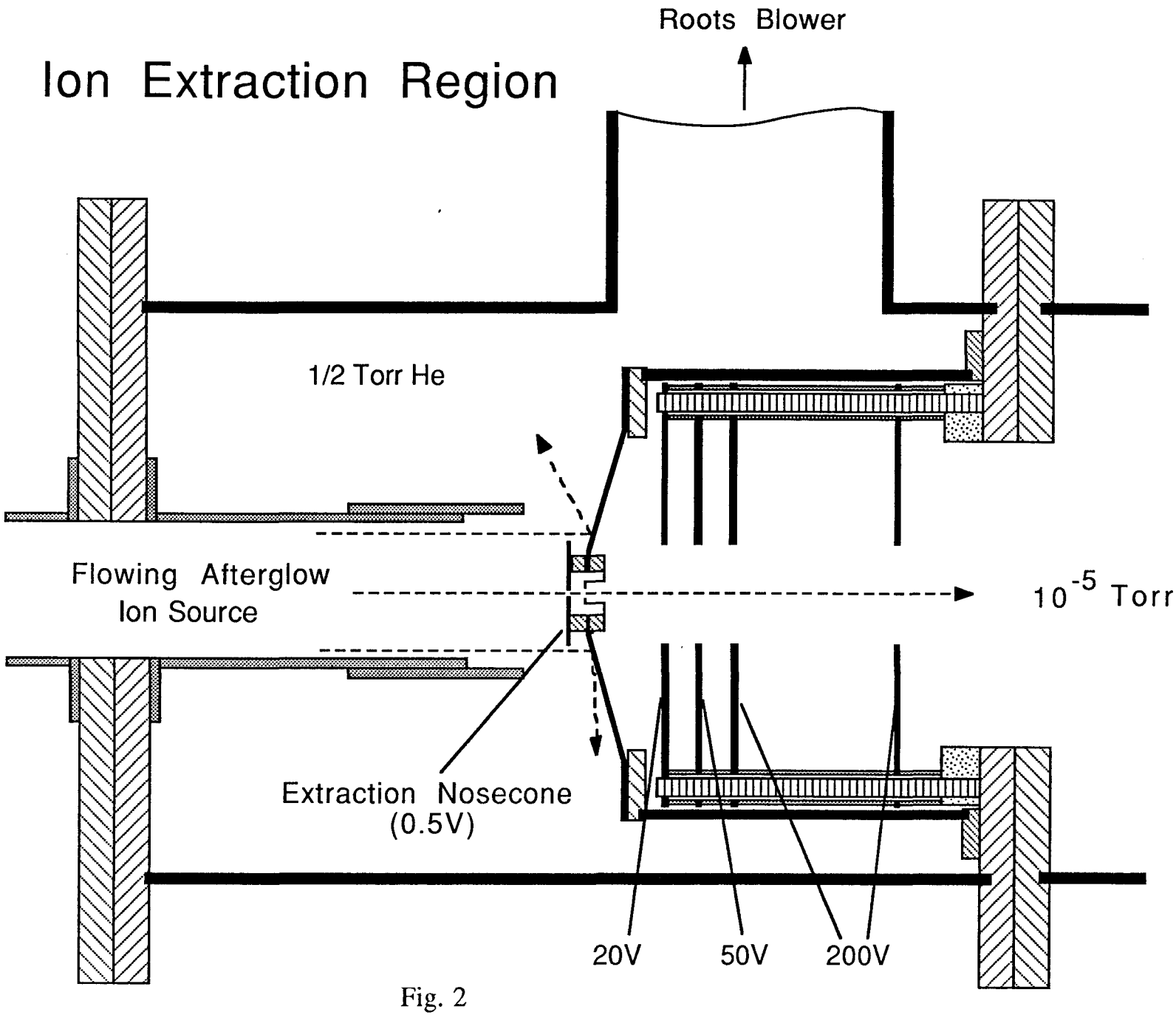
Roots Blower
Ion Extraction Region
1/2 Torr He
Flowing Afterglow
Ion Source
10^{-5} Torr
Extraction Nosecone
(0.5V)
20V
50V
200V

Fig. 2

Ions are swept down the flow tube of the afterglow and exhausted by a large Roots pump. This nosecone has a molybdenum disc with a 1 mm aperture as the sampling element. Suppose one has a negative ion density of 10^9 cm^{-3} immediately before the molybdenum disc; the current of ions sampled by the nosecone (indicated by the dotted line) will be roughly 2×10^{10} sec^{-1} or about 2 nA. Of course, these ions are entrained in a helium buffer gas at about 0.5 Torr (10^{16} atoms cm^{-3}) and a major task is to extract the negative ions from the neutral buffer gas and form them into an ion beam.

In order to avoid collisionally exciting the ions as they are extracted, the lens voltages must be held at low values. Elements in the extraction region will be in the range of 1 V or less since the helium number density will be rather high at precisely this point. If one uses large voltages right here, there is a real danger of collisionally exciting the ions as they are extracted. Further down the extraction region, a set of four lens elements at 20 V, 50 V and 200 V accelerate and focus the ions into a large einzel lens. The goal of the devices in Fig. 7 is to extract ion beams with a current of $\cong$ 1 nA from the afterglow source with a minimum of collisional excitation, accelerate them up to several hundred volts and deliver them to the Wien filter for mass-selection.

(ii) Wien Velocity Filter

Following extraction and acceleration to 600 eV, the ions are velocity selected by a 6 in. Wien filter (Colutron 600-B). Since all of the ions have a nominal kinetic energy of 600 eV, velocity selection amounts to mass selection. The mass-selected ions pass through a field-free drift region (1.5 m) to increase their spatial dispersion and then impinge on a $\frac{1}{2}$ mm slit, which separates the mass selection and laser interaction regions. The expected mass resolution of this device is 585. Passing through the knife edges of the slit, the mass-selected ion beam enters a 5-element deceleration lens (Colutron 400-L) situated immediately before the ion/laser intersection turret. The function of this lens is to slow the ion beam from 600 eV to roughly 20 eV without loss of beam current. The residence time

of the ions in the radiation field of the laser is thus increased by a factor of $\sqrt{30}$ and we anticipate a concomitant increase in the photodetachment signal.

(iii) New Electron Energy Analyzer

Our original photoelectron spectrometer utilized a pair of 1 in. mean radius hemispherical analyzers arranged in series. We routinely achieved an operating resolution of approximate 20 meV but this spectrometer is very insensitive. We require beam currents of 100 pA or greater to carry out a study; 100 pA currents are barely suitable and nA currents are much more tractable. If we have any hope of using ions from a flowing afterglow ion source, we must be able to deal with mass-selected beam currents in the range of 10 pA.

We have just completed the construction of a new electron energy analyzer whose sensitivity makes possible the incorporation of a flowing afterglow ion source into our apparatus. As show schematically in Fig. 3, our new instrument features a single, large 3 in. mean radius hemispherical analyzer outfitted with a position-sensitive detector. In addition to a dramatic increase in sensitivity, we expect an increase in the resolution of our electrostatic analyzer to about 5 meV FWHM.

A key feature of our new analyzer is an improved set of electron lenses (Fig. 4) which is designed to provide us with most of our sensitivity increase. The input lens stack accelerates electrons possessing a particular kinetic energy in the range of the laser (0 to 2.540 eV) up to the transmission energy (T_o) of the analyzer while imaging these electrons at the entrance plane of the hemispheres. The lens stack is composed of a molybdenum turret (IR) (where the ion and laser beams intersect) and four OFHC cylinders (LI1-LI4) with inner diameters (D) of $\frac{3}{8}$ in. and gaps of 0.0375 in.

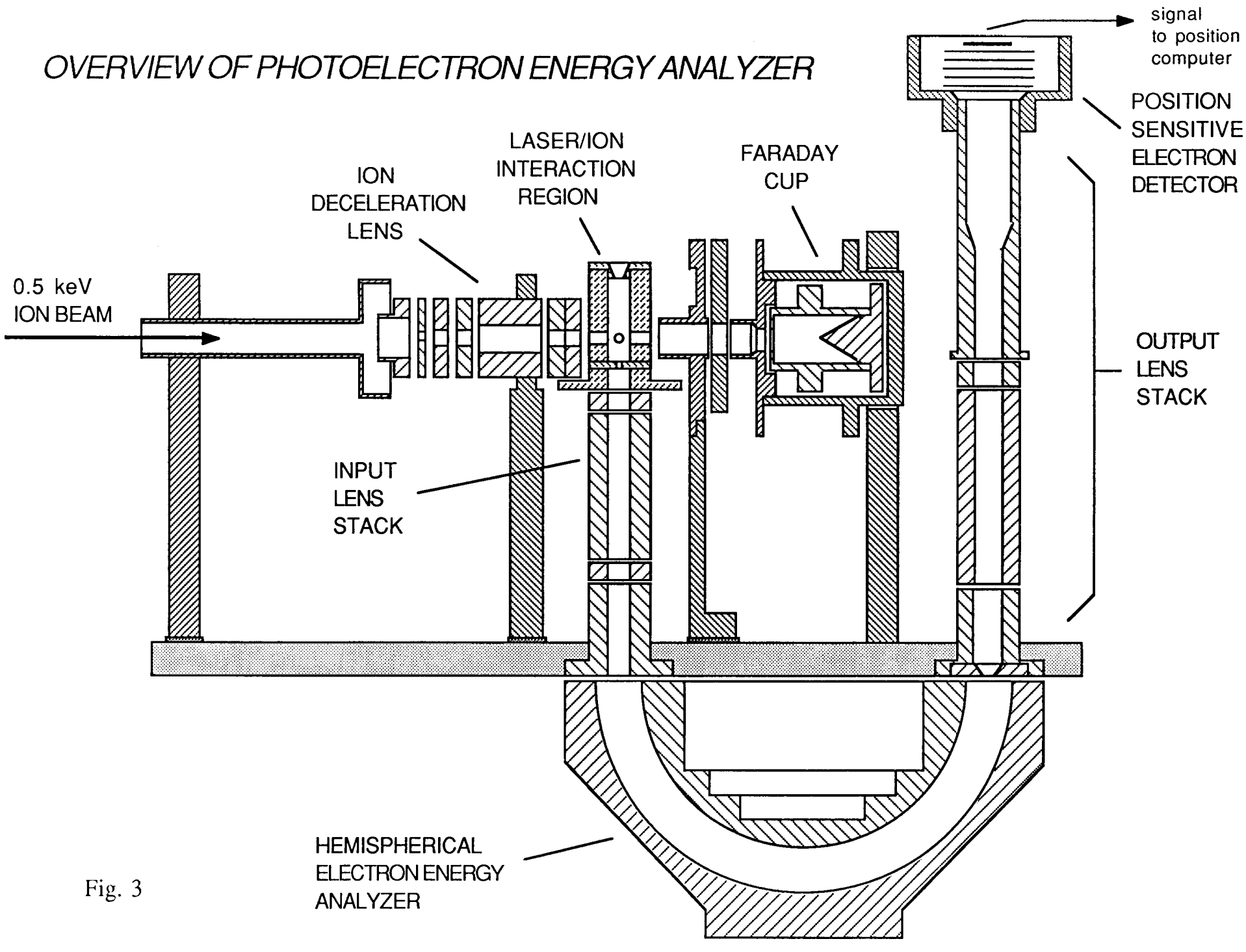
OVERVIEW OF PHOTOELECTRON ENERGY ANALYZER
signal
to position
computer
POSITION
SENSITIVE
ELECTRON
DETECTOR
LASER/ION
INTERACTION
REGION
FARADAY
CUP
ION
DECELERATION
LENS
0.5 keV
ION BEAM
OUTPUT
LENS
STACK
INPUT
LENS
STACK
HEMISPHERICAL
ELECTRON ENERGY
ANALYZER

Fig. 3

DIAGRAM OF THE ANALYZER LENS SYSTEM

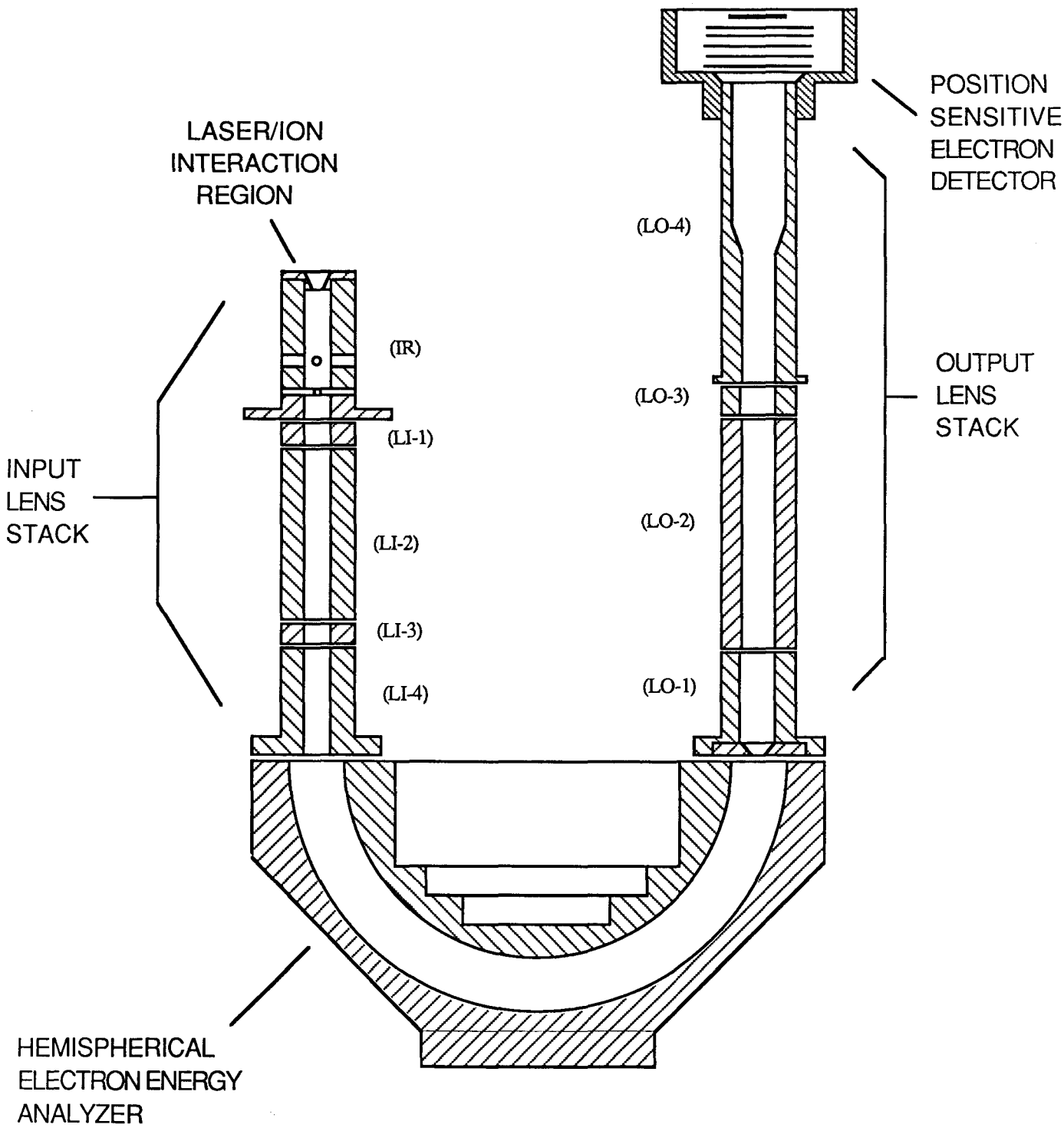

Fig. 4

These set of five pieces constitutes a pair of 3-element zoom lenses where element LI2 is common to both. The first lens (elements IR-LI2) operates as a fixed accelerator (x10) to minimize the effects of irregular E-fields on the relatively slow-moving detached electrons. The second lens (elements LI2-LI4) then accelerates/decelerates electrons of the appropriate energy (varied during a scan) to an energy T_0 as they enter the hemispheres. Element LI-4, commonly referred to as a Herzog corrector, is designed to effect a smooth transition between the input lens stack and the hemispherical analyzer by minimizing penetration of the radially varying electric field of the hemispheres into the essentially field-free region in the end of lens element LI-4. Two aspects of this input lens stack make our new analyzer much more sensitive than the old one. These are (a) the precise imaging capabilities of the input lens stack makes a physical slit at the entrance to the hemispheres unnecessary. And (b) a 0.065 in. aperture at the bottom of the molybdenum interaction region element (IR) defines a half-angle of acceptance (5^o) which is larger than that of the old analyzer (3^o). This represents an increase in angular acceptance, and therefore in sensitivity, of $\frac{25}{9}$.

Our hemispherical electrostatic analyzer, sketched in Figs. 3 and 4, consists of concentric OFHC hemispheres having a mean radius of 3 in. and a gap of $\frac{3}{4}$ in. These hemispheres were carefully machined to achieve a sphericity tolerance of $\pm$ 0.001 in. and a surface finish of 16 μin. They were then treated with a colloidal suspension of graphite (Aerodag-G) to improve their surface electrical properties. Voltages are applied to the hemispheres to set up an electric field directed radially inward. Electrons entering the hemispheres with kinetic energy T are dispersed by this field along the radial coordinate by a distance proportional to $(T-T_0)$, where T_0 is the transmission energy of the analyzer, typically 1-5 volts. This analyzer is expected to have an operating resolution of 5 meV, a factor of 4 improvement over our old analyzer.

The output lens stack serves to magnify the spatial dispersion of the electrons exiting the hemispheres to match the physical dimensions of the position-sensitive detector.

It also accelerates the electrons to an energy where the electron detection efficiency is high ($\cong$ 300 eV). We use a Surface Science Laboratories Model 3391 Open Face Sensor together with the accompanying Model 2401 Position Computing Electronics to detect the energy analyzed electrons. The detector has two stages of operation. The first phase is charge amplification in which the incoming electrons are amplified by roughly 10^8 with a stack of five 25 mm Varian microchannel plates. The amplified electrons then impinge on the 25 mm resistive anode. The position of the charge burst on the anode is determined by a principle of charge division. The pulse of electrons strikes the anode and spreads out isotropically. Four electrodes located at the corners of the anode measure the capacitance at each corner. By taking the appropriate sums and ratios of the charge collected at each electrode, the position computing electronics outputs two 0-4 volt signals which represent the X and Y coordinates of the location where the electron struck the detector. These two signals are digitized and sent to the host computer for storage. The multichannel nature of this detector translates into a collection energy bandwidth of 150-200 meV. In comparison, a traditional Ceratron type of detector would have a bandwidth of about 5 meV.

REFERENCES

1 C.T. Wickham-Jones, S. Moran, and G.B. Ellison, J. Chem. Phys. **90**, 795 (1989).

2 C.T. Wickham-Jones, K.M. Ervin, G.B. Ellison, and W.C. Lineberger, J. Chem. Phys. **91**, 2762 (1989).

3 K.C. Symth and J.I. Brauman, J. Chem. Phys. **56**, 4620 (1972).

4 R.J. Celotta, R.A. Bennett and J.L. Hall, J. Chem. Phys. **60**, 1740 (1974).

5 M.W. Siegel, R.J. Celotta, J.L. Hall, J. Levine, and R.A. Bennett, Phys. Rev. A **6** (1972) 607.

6 R.J. Celotta, R.A. Bennett, J.L. Hall, M.W. Siegel, and J. Levine, Phys. Rev. A **6** (1972) 631.

7 M.J. Travers, D.C. Cowles, and G. Barney Ellison, Chem. Phys. Letts (in press, 1989).

8 D. Golden and McMillen, Annu. Rev. Phys. Chem. **33**, 493 (1982).

9 D.G. Leopold, K.K. Murray, A.E. Stevens Miller, and W.C. Lineberger, J. Chem. Phys. **83**, 4849 (1985).

10 (a) R. Walsh, Acc. Chem Res. **14**, 246 (1981); (b) P.N. Noble and R. Walsh, Int. J. Chem. Kinetics **15**, 547 (1983); (c) J. Berkowitz, J. Chem. Phys. **89**, 7065 (1988), Table III.

11 Ionization potentials and electron affinities are strictly changes of enthalpy at 0 °K, while ΔH^{o}_{acid} is the the enthalpy change for (1) at 298 °K. Equation (3) is more properly written as:

$$\Delta H^{o}_{acid}(R\text{-}H) = D_{298}(R\text{-}H) + IP(H) - EA(R) + \langle \Delta C_p \rangle_0^{298}.$$

The difference in the integrated heat capacities can be written in the following manner: $\langle \Delta C_p \rangle_0^{298} \equiv \langle C_p^o(T)[R^-] - C_p^o(T)[R] \rangle_0^{298} + \langle C_p^o(T)[H^+] - C_p^o(T)[H] \rangle_0^{298}$. In most cases the heat capacity correction is less than 0.5 kcal/mol since the structures and vibrational frequencies of the ions and neutrals are similar. Because the uncertainties of the ΔH^{o}_{acid} measurements are commonly ± 2 kcal/mol or greater, this correction is usually ignored; thus $\langle \Delta C_p \rangle_0^{298} \cong 0$ kcal/mol. (See Lias *et al.* ref. 12, § 3.3).

12 S.G. Lias, J.E. Bartmess, J.F. Liebman, J.L. Holmes, R.D. Levin, and W.G. Mallard, Gas-Phase Ion and Neutral Thermochemistry, J. Phys. Chem. Reference Data, **17**, Supplement No. 1 (1988).

13 M.W. Chase Jr., C.A. Davies, J.R. Downey,Jr., D.J. Frurip, R. A. McDonald, A. N. Syverud,*J. Phys. Chem. Ref. Data* **1985**, *14* (Supplement 1).

14 K.M. Ervin, G.B. Ellison, M.K. Gilles, A.G. Harrison, S.E. Barlow, S. Gronert, V.M. Bierbaum, W.C. Lineberger, and C.H. DePuy, J. Amer. Chem. Soc. (submitted, 1989).

15 D.G. Leopold, K.K. Murray, A.E. Stevens Miller, and W.C. Lineberger, J. Chem. Phys. **83**, 4849 (1985).

16 H.B. Ellis Jr. and G.B. Ellison, J. Chem. Phys. **78** 6541 (1983).

17 H.B. Ellis Jr., PhD Thesis, University of Colorado (1983).

18 E.E. Ferguson, F.C. Fehsenfeld, and A.L. Schmeltekopf, Adv. Atom. Molec. Phys. **6**, 1 (1969); S.T. Graul and R.R. Squires, Mass Spectrometry Revs. **7**, 263 (1988).

19 Mark E. Jones and G.B. Ellison, Rev. Sci. Instrum. **57**, 1432 (1986).

20 J. Van Doren, C.H. DePuy, and V.M. Bierbaum, privately communicated (1986).

21 D. Smith and N.G. Adams, J. Phys. D **13** 1267 (1980).

reprints + preprints removed.
ds